Letters

Optimum Design of Wireless Power Transfer-Based Snubbers for SiC MOSFET Switching Oscillations

Bowang Zhang, Wei Han, *Member, IEEE*, Binhong Cao, Weikang Hu, *Graduate Student Member, IEEE*, and Youhao Hu

***Abstract*—This letter proposes a novel wireless power transfer (WPT)-based snubber circuit aimed to suppress the ringing of SiC MOSFET resulting from parasitic impedances in the switching circuit. The key innovation lies in the artful transfer of the ringing energy to an optimally designed receiver via magnetic resonant coupling. It reveals that the oscillation time of switching ringing can be reduced by up to 67%, significantly expanding the upper limit of the switching frequency and reducing electromagnetic interference. Compared to the traditional RC snubber, permissible voltage and energy loss of the WPT snubber is reduced by 87.84% and 86.84%. This technology greatly reduces the sizes of passive components, resulting in a huge enhancement of power density. Finally, both theoretical analyses and experimental results confirm the effectiveness of the proposed system.**

***Index Terms*—Electromagnetic interference (EMI), power density, switching oscillation, WPT snubber.**

TABLE I
COMPARISON BETWEEN *RC* AND WPT SNUBBER CIRCUITS

Feature	*RC snubber*	*WPT snubber*
Electrical isolation	No	Yes
Switching loss of R_{snb}	High	Low
Permissible voltage of C_{snb}	High	Low
Power density	Low	High
Cost	High	Low
Energy recycling	Hard	Easy

I. INTRODUCTION

SIC MOSFETs are increasingly favored in applications that require rapid and efficient switching. However, the capability for fast switching results in high dv/dt, and when this is combined with the stray inductance from packaging and surrounding circuitry, it leads to significant surge voltage between the drain and source of the MOSFET [1]. This surge voltage needs to be carefully managed so as not to exceed the maximum rated voltage of the devices. To dampen the ringing phenomenon, passive *RC* snubber circuits have been conventionally employed [2]. The key is to insert a capacitor and resistor in parallel with the switching device, in which ceramic capacitors are commonly utilized due to their high capacitance values. Nonetheless, the risk of the short-circuit current flowing through the power lines exists in the event of a capacitor malfunction [3]. In addition, as the power level and bus voltage increase, the size of the *RC* snubber circuit will significantly expand, severely limiting the power density of the converter.

The magnetic resonant coupling-based wireless power transfer (WPT) inherently possesses the ability to conduct ac while blocking dc [4]. When integrated with a snubber circuit, it can effectively transfer high-frequency ac ringing energy without affecting dc components of the surge voltage. Consequently, a novel WPT snubber circuit is proposed to deliberately suppress the ringing issue with the features of electrical isolation, high power density, low cost, and energy regeneration, as listed in Table I. The novelty of the proposed WPT snubber circuit can be summarized as follows.

1) The inherent electrical isolation characteristics eliminates the short-circuit risk of MOSFET switch resulting from any malfunction of the traditional snubber capacitor.
2) The WPT snubber circuit will completely prevent the high dc component of the primary side switching voltage from being transmitted to the secondary side, thus freeing the secondary snubber resistor and capacitor from handling the dc bias voltage.
3) Only low-power resistor and low-voltage capacitor are required to handle the ringing energy and voltage. That not only reduces the overall volume but also results in cost savings. Besides, energy recycling is possible by capturing the ringing energy and feeding it back to the auxiliary power supply of driver circuit.

Manuscript received 7 March 2024; revised 12 April 2024 and 25 May 2024; accepted 27 May 2024. Date of publication 18 June 2024; date of current version 16 July 2024. This work was supported in part by Guangdong Basic and Applied Basic Research Fund under Grant 2022A1515110410 and in part by Guangzhou-HKUST(GZ) Joint Funding Program under Grant 2024A03J0618. *(Corresponding author: Wei Han.)*

The authors are with the Sustainable Energy and Environment Thrust, The Hong Kong University of Science and Technology, Guangzhou 511453, China (e-mail: bzhang794@connect.hkustgz.edu.cn; weihan@hkust-gz.edu.cn; binhongcao@hkust-gz.cn; yhu543@connect.hkust-gz.edu.cn).

Color versions of one or more figures in this article are available at https://doi.org/10.1109/TPEL.2024.3415741.

Digital Object Identifier 10.1109/TPEL.2024.3415741

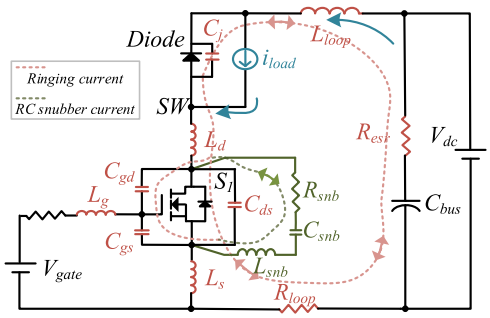

Fig. 1. Double pulse test circuit considering parasitic components with a *RC* snubber circuit.

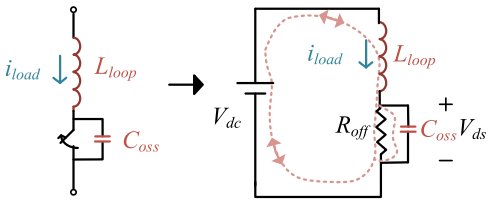

Fig. 2. Equivalent circuit when S_1 turns OFF.

II. Analysis of Switching Ringing and Snubber Circuit

A. Analysis of MOSFET Switch Ringing

As depicted in Fig. 1, upon activation of a MOSFET, partial energy will be stored in the stray inductance L_{loop} of the wire within the PCB layout due to the current i_{load}. The stored energy then resonates with the parasitic capacitor C_{oss} (C_{ds}+C_{gd}) of the MOSFET and the total capacitance C_j of diode, generating the ringing phenomenon. Hence, the trajectory of ringing current and *RC* snubber current are illustrated in the double pulse test circuit, which consists of a diode, a load inductor L_{load} and a MOSFET switch S_1.

When S_1 turns OFF, i_{load} flows through the loop formed by L_{loop}, C_{bus}, R_{esr}, C_j, and S_1, as indicated by the dotted red line. The deactivation of S_1 incites a surge voltage in the drain-source, a result of the resonant phenomenon between L_{loop} and the parasitic capacitance C_{oss} of S_1. Hence, Fig. 2 illustrates the equivalent circuit when S_1 turns OFF, where R_{off} represents the turn-OFF resistance.

Based on the Kirchhoff's current law (KCL) and Kirchhoff's voltage law (KVL) theorems, a set of differential can be formulated as follows:

$$\left.\begin{aligned} L_{\text{loop}}\tfrac{di_{\text{load}}}{dt}+V_{ds}&=V_{\text{dc}}\\ i_{\text{load}}&=C_{\text{oss}}\tfrac{dV_{ds}}{dt}+\tfrac{V_{ds}}{R_{\text{off}}}\end{aligned}\right\}. \tag{1}$$

The initial conditions are indicated by (2), which I_{load} is constant current load

$$\left.\begin{aligned} i_{\text{load}}(0)&=I_{\text{load}}\\ V_{ds}(0)&=0\end{aligned}\right\}. \tag{2}$$

The solution to (1) yields the surge voltage V_{ds} as follows:

$$V_{ds}=V_Ae^{-\alpha t}\sin(\omega t-\phi)+V_{\text{dc}} \tag{3}$$

$$\left.\begin{aligned} V_A&=\sqrt{V_{\text{dc}}^2+(\alpha/\omega)^2(2R_{\text{off}}I_{\text{load}}-V_{\text{dc}})^2}\\ \phi&=\tan^{-1}\tfrac{V_{dc}}{(\alpha/\omega)(2R_{\text{off}}I_{\text{load}}-V_{\text{dc}})}\\ \alpha&=\tfrac{1}{2R_{\text{off}}C_{\text{oss}}}\\ \omega&=\tfrac{1}{\sqrt{L_{\text{loop}}C_{\text{oss}}}}\sqrt{1-\left(\tfrac{\sqrt{L_{\text{loop}}/C_{\text{oss}}}}{2R_{\text{off}}}\right)^2}\ \left(\sqrt{\tfrac{L_{\text{loop}}}{C_{\text{oss}}}}\le 2R_{\text{off}}\right)\end{aligned}\right\}. \tag{4}$$

Therefore, the peak value of V_{ds}, representing the voltage stress on the switch, can be denoted as V_p and calculated by

$$V_p=\frac{V_Ae^{-(\alpha/\omega)[\tan^{-1}(\alpha/\omega)+\phi]}}{1+(\alpha/\omega)^2}+V_{\text{dc}}. \tag{5}$$

B. RC Snubber Circuit

The green dashed line in Fig. 1 illustrates the current loop when the *RC* snubber circuit works, where the C_{snb} will absorb the energy stored at L_{loop}. In order to achieve optimal snubber performance, it is crucial for the C_{snb} to be sufficiently large to retain energy and prevent unexpected discharging. It is important to note that the equivalent series inductance of the L_{snb} cannot be overlooked given its large size. However, the stray inductance L_{snb} of the snubber path is still much smaller than the load inductance L_{loop}.

Prior to *RC* snubber design, it is essential to determine C_{oss} and L_{loop}. According to (4), the frequency of switching oscillation without a snubber f_{ringing} can be calculated as follows:

$$f_{\text{ringing}}=\frac{\omega}{2\pi}=\frac{1}{2\pi\sqrt{L_{\text{loop}}C_{\text{oss}}}}\sqrt{1-\left(\frac{\sqrt{L_{\text{loop}}/C_{\text{oss}}}}{2R_{\text{off}}}\right)^2}\times\left(\sqrt{\frac{L_{\text{loop}}}{C_{\text{oss}}}}\le 2R_{\text{off}}\right). \tag{6}$$

The value of f_{ringing} can be accurately determined through measurement, and when combined with C_{oss} from the datasheet of S_1, L_{loop} can be calculated using (6).

If C_{snb} is replaced with a short circuit, the equivalent circuit when S_1 turns OFF becomes approximately the *RLC* circuit. Define the damping ratio ζ as follows:

$$\zeta=\frac{1}{2R_{\text{snb}}}\sqrt{\frac{L_{\text{loop}}}{C_{\text{oss}}}}\rightarrow R_{\text{snb}}=\frac{1}{2\zeta}\sqrt{\frac{L_{\text{loop}}}{C_{\text{oss}}}}. \tag{7}$$

Theoretically, the circuit will oscillate indefinitely if $\zeta=0$. However, this is practically impossible due to the presence of resistance in a real circuit. As ζ approaches one, the oscillation becomes more damped, meaning it tends to decrease over time with an exponential decay envelope. This is referred to as an "underdamped" response. When $\zeta=1$, it is considered "critically damped" and at this point, oscillation ceases. For values greater than one (overdamped), the response of circuit becomes more sluggish, with the waveform taking longer to reach its final value. So set $\zeta=1$ and solve for R_{snb}.

However, in typical half-bridge circuits, S_1 would be permanently shorted by the resistor and the circuit as a whole would not operate as required, if there is only a resister R_{snb}. The solution is therefore to place C_{snb} in series with R_{snb}. Define the cutoff

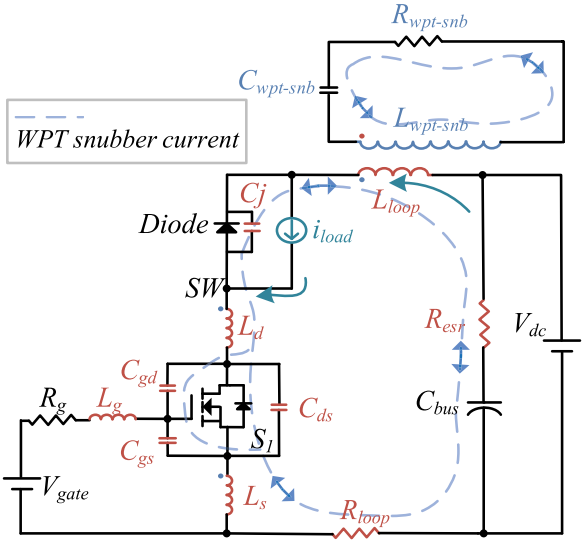

Fig. 3. Double pulse test circuit with the proposed WPT snubber circuit.

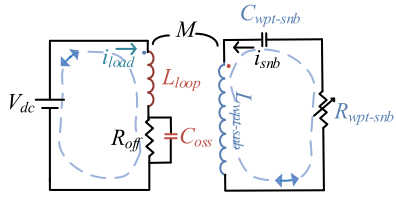

Fig. 4. Equivalent circuit with the proposed WPT snubber circuit.

frequency f_c as follows:

$$f_c = \frac{1}{2\pi R_{\text{snb}} C_{\text{snb}}} \rightarrow C_{\text{snb}} = \frac{1}{2\pi R_{\text{snb}} f_c} = \frac{\zeta}{\pi f_c}\sqrt{\frac{C_{\text{oss}}}{L_{\text{loop}}}}. \quad (8)$$

The selection of the appropriate value for f_c is crucial. The cutoff frequency of the *RC* snubber should be sufficiently low to effectively suppress the undamped oscillation frequency f_{ringing}, while also avoiding a significant conduction path at the operating frequency of circuit. A good choice is often $f_c = f_{\text{ringing}}$, which will resolve for C_{snb} [5].

After setting R_{snb} and C_{snb}, their sizes should be determined based on the power dissipation calculated by (9), which implies that the total energy stored by the parasitic inductance L_{loop} and snubber capacitor C_{snb} in the loop will be ultimately dissipated in the snubber resistor R_{snb}

$$P_{\text{snb}} = C_{\text{snb}} V_{\text{dc}}^2 f_{\text{sw}}. \quad (9)$$

This equation reveals that an increase in either the switching frequency f_{sw} or V_{dc} will result in a corresponding increase in the power dissipation demands for R_{snb}. If the power dissipation P_{snb} exceeds the resistor's capacity, it becomes necessary to decrease the capacitance of C_{snb} accordingly.

C. WPT Snubber Circuit

As shown in Fig. 3, the ringing voltage, PCB parasitic inductor and a specially designed coil can be regarded as the ac input voltage, primary coil and secondary coil in a WPT snubber circuit, respectively, and this can be simplified by an equivalent circuit as depicted in Fig. 4, in which the key is to optimize the $C_{\text{wpt-snb}}$ to form the magnetic resonant coupling and adjust the value of $R_{\text{wpt-snb}}$ to achieve maximum suppression ratio of ringing from the primary side.

According to Kirchhoff's law and Ohm's law, the following set of equations can be obtained as:

$$\left.\begin{aligned} &L_{\text{loop}}\tfrac{di_{\text{load}}}{dt} + V_{ds} + M\tfrac{di_{\text{snb}}}{dt} = V_{\text{dc}} \\ &i_{\text{load}} = C_{\text{oss}}\tfrac{dV_{ds}}{dt} + \tfrac{V_{ds}}{R_{\text{off}}} \\ &L_{\text{wpt - snb}}\tfrac{di_{\text{snb}}}{dt} + M\tfrac{di_{\text{load}}}{dt} + V_{C_{\text{wpt - snb}}} + R_{\text{wpt - snb}} i_{\text{snb}} = 0 \\ &V_{C_{\text{wpt - snb}}} = \tfrac{1}{C_{\text{wpt - snb}}}\int i_{\text{snb}} dt \end{aligned}\right\}. \quad (10)$$

The initial conditions of (10) are indicated by

$$\left.\begin{aligned} i_{\text{load}}(0) &= I_{\text{load}} \\ V_{ds}(0) &= 0 \end{aligned}\right\}. \quad (11)$$

Given that the (10) lacks an analytical solution and only permits a numerical one, the time-domain expression (12) derived by inverse Laplace transform serves as a general solution with undetermined constants

$$V_{ds} = pe^{-\varepsilon t}\sin(\omega_p t - \phi_p) + se^{-\delta t}\sin(\omega_s t - \phi_s) + V_{\text{dc}}. \quad (12)$$

The presence of two voltages with different frequencies (ω_p and ω_s) in the ringing voltage V_{ds} indicates frequency splitting under strong coupling, where the two frequencies tend to natural resonant frequency as the coupling coefficient decreases [6]. Their combination accordingly causes oscillatory waveforms to decay and exhibit varying envelope shapes. Following the principle of magnetic resonance in a WPT system, capacitor $C_{\text{wpt-snb}}$ can be carefully adjusted to make secondary resonant frequency equal to the primary resonant frequency. Since the primary damping ratio is constant, the overall duration of ringing can be flexibly adjusted by changing the secondary side damping ratio, namely, adjusting $R_{\text{wpt-snb}}$. Hence, based on (12), the maximum reduction for the duration of switching ringing can be readily achieved by mathematically determining the optimal parameters in the WPT snubber circuit.

III. Experimental Verification

Fig. 5 depicts a double pulse test setup with the WPT snubber circuit. This platform with WPT snubber circuit, controlled by DSP (TMS320F28027), includes components, such as busbar, inductor load, switch S_1 (1V1Q12050T3), silicon carbide diode (STPSC10H12) and WPT-based snubber with full-wave rectifier. The WPT snubber circuit proposed in this letter utilizes a planar PCB coil structure and can be integrated into a dual pulse test board. Fig. 5 illustrates an expansion of the plate spacing by ten times, clearly showing that the fourth and fifth layers out

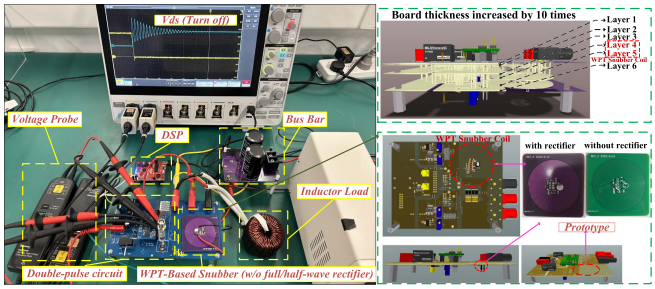

Fig. 5. Experimental setup of double pulse test integrated with the WPT snubber circuit (w/o full/half-wave rectifier).

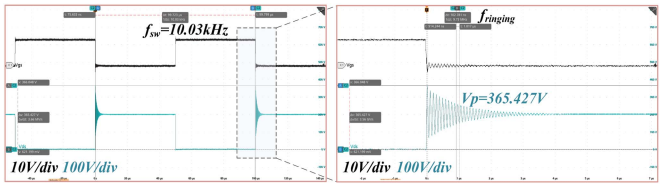

Fig. 6. Switching waveform of V_{ds} without snubber circuits.

TABLE II
CRITICAL PARAMETERS

Item	Value	Item	Value
C_{oss}	110 pF	f_{sw}	10 kHz
R_{off}	300 Ω	L_{load}	500 μH
L_{loop}	2.43 μH	V_{dc}	200 V
$L_{wpt\text{-}snb}$	180 μH	$C_{wpt\text{-}snb}$	1.5 pF
C_{bus}	1360 μF	Cj	47 pF

of six are WPT snubber coils. The low-power resistor and low-voltage capacitor of the WPT snubber can be encapsulated in SMD0805 at Layer 1, facilitating parameter adjustment without increasing volume. The oscilloscope captures the waveform of the ringing voltage V_{ds} that arises when S_1 is turned OFF. The specifications for the chosen switch S_1 indicate the parasitic capacitance C_{oss} and the OFF-state resistance R_{off}. When S_1 operates at the frequency f_{sw}, the measured waveform of V_{ds} reveals that the ringing frequency f_{ringing} and maximum voltage V_p are around 10.2 MHz and 365.427 V, respectively, as depicted in Fig. 6. Once values of f_{ringing}, R_{off} and C_{oss} are known, the parasitic inductance L_{loop} can be calculated by using (4) and the inductance of specifically-designed PCB coil can be measured. Finally, the secondary capacitor $C_{\text{wpt-snb}}$ can be determined to achieve an identical resonance frequency for both primary and secondary sides. The critical parameters are summarized in Table II.

Once determining the values of $L_{\text{wpt-snb}}$ and $C_{\text{wpt-snb}}$, it is crucial to design an optimal $R_{\text{wpt-snb}}$ to effectively suppress ringing. Consequently, Fig. 7 demonstrates the impact of the damping of switching ringing when S_1 is turned OFF, with $R_{\text{wpt-snb}}$ values of 4, 6, 10, and 16 Ω, respectively. The gray waveform represents switch ringing without snubber circuits and serves as a baseline for comparison. The inclusion of the WPT snubber circuit significantly shortens the ringing, as shown by the blue line overlapping the gray line. Besides, the voltage

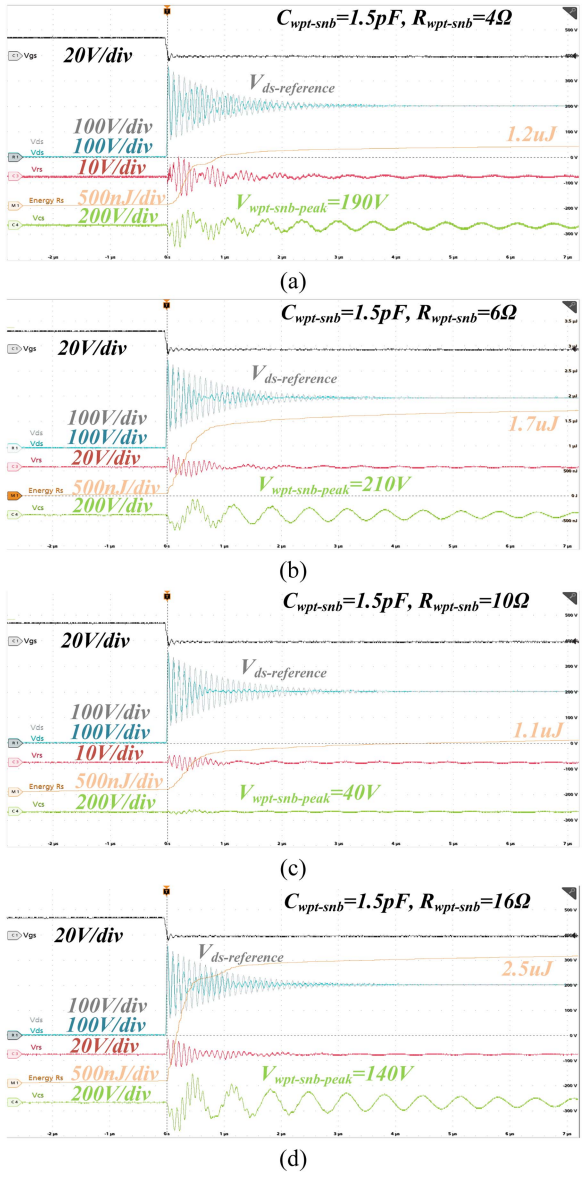

Fig. 7. Experimental waveforms of $V_{ds\text{-reference}}$, V_{ds}, $V_{C\text{wpt-snb}}$, $V_{R\text{wpt-snb}}$, and energy loss of $R_{\text{wpt-snb}}$. (a) $R_{\text{wpt-snb}} = 4\ \Omega$. (b) $R_{\text{wpt-snb}} = 6\ \Omega$. (c) $R_{\text{wpt-snb}} = 10\ \Omega$. (d) $R_{\text{wpt-snb}} = 16\ \Omega$.

waveforms across $C_{\text{wpt-snb}}$ and $R_{\text{wpt-snb}}$ are depicted in green and red lines, respectively, and the orange curve represents the cumulative energy dissipated by $R_{\text{wpt-snb}}$ during the turn-OFF period of S_1.

With adoption of WPT snubber circuit, it can be observed that the oscillation time of ringing varies with different $R_{\text{wpt-snb}}$ values as depicted in Fig. 7. Fig. 8 demonstrates that the absence of any snubber circuit exacerbates the electromagnetic interference (EMI) issue, whereas the implementation of the WPT snubber circuit and setting $R_{\text{wpt-snb}}$ to 10 Ω leads to the most significant reduction in EMI emissions. Select the peak points in the extended Fig. 8, where blue and red point (f_{low} *and* f_{high}) represent less and greater than natural resonant frequency f_{ringing} (gray point), respectively. The yellow star-shaped marker $f_{\text{res(ep)}}$ indicates the critical point for frequency splitting. It can

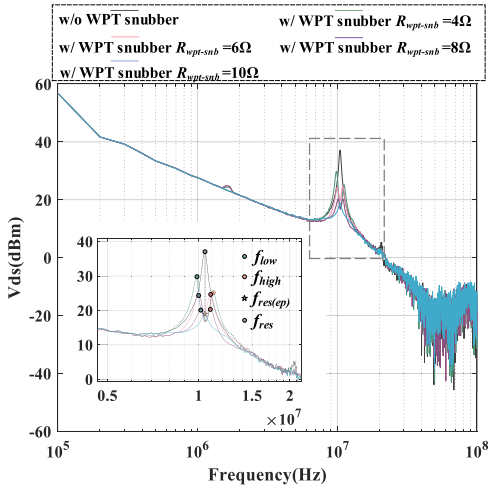

Fig. 8. Frequency spectrum of V_{ds} (w/o WPT snubber).

be seen that as $R_{\text{wpt-snb}}$ increases, the frequency composition of the ringing gradually tends from two splitting frequencies towards the same frequency f_{ringing}. This phenomenon can be attributed to the rightward movement of the exceptional point (EP) point caused by increased load, which compels the critical coupling to approach the actual coupling strength of the circuit [6]. At the critical point of frequency splitting, it exhibits the excellent characteristics of having the minimum permissible voltage of $C_{\text{wpt-snb}}$ and power dissipation of $R_{\text{wpt-snb}}$, which is the optimal design point for $R_{\text{wpt-snb}}$.

Furthermore, Fig. 9 shows that the optimal $R_{\text{wpt-snb}}$ corresponds to the critical point for frequency splitting of switch ringing. When the $R_{\text{wpt-snb}}$ is high, the ringing frequency aligns with the natural resonant frequency on the primary side. When the $R_{\text{wpt-snb}}$ is low, the ringing frequency will be reduced accordingly. It should be noted that this rule can greatly simplify the process of determining the optimal $R_{\text{wpt-snb}}$. Finally, Fig. 10 presents a flowchart that enables the rapid design of critical parameters for a WPT snubber circuit, effectively simplifying the intricate task of measuring parasitic parameters and deducing mathematical equations. The $f_{\text{wpt-ringing}}$ indicates the frequency of the switch ringing to be measured as the WPT snubber is used. The value of $f_{\text{wpt-riging}}$ will vary with different WPT snubber parameters. The proposed optimal design method of WPT snubber circuit in this letter can efficiently address the following issues: the difficulty in accurately measuring the parasitic parameters of the switch and the system, as well as the challenge of accurately modeling the distributed parasitic inductance L_{loop}.

As depicted in Fig. 11, the ringing suppression effects of *RC* snubber and WPT snubber are compared. The optimal parameters of $R_{\text{snb}} = 74.31\ \Omega$, $C_{\text{snb}} = 209$ pF, and E_{snb} (switching energy loss of R_{snb}) $= 8.36\ \mu$J are calculated based on the experimental data in Table II and formula (7)–(9). The experimental results in Fig. 7 indicate that the E_{snb} of WPT snubber with parameter optimization is 1.1μJ. While both WPT and *RC* snubbers can effectively inhibit ringing, *RC* snubber demonstrates superior inhibition. Specifically, *RC* snubber reduces ringing to

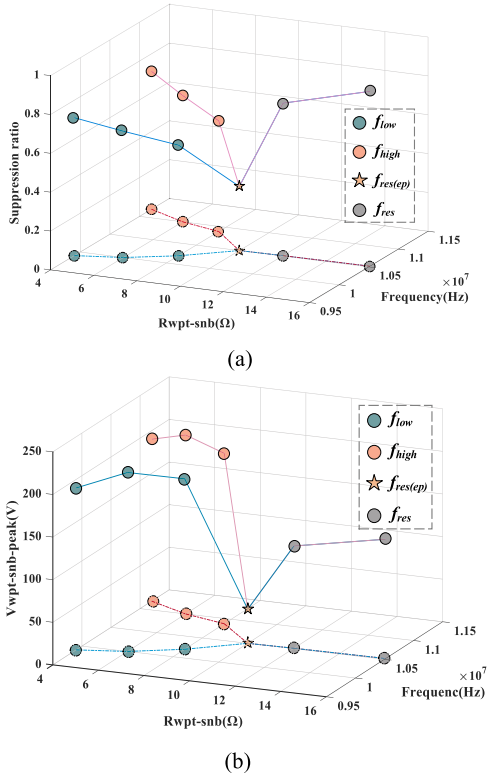

Fig. 9. Curve graphs of (a) suppression ratio; (b) $V_{\text{wpt-snb-peak}}$ as $R_{\text{wpt-snb}}$ and $f_{\text{wpt-ringing}}$ varies.

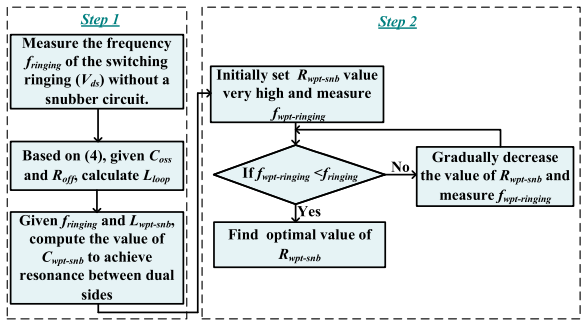

Fig. 10. Proposed design procedure for WPT snubber circuit.

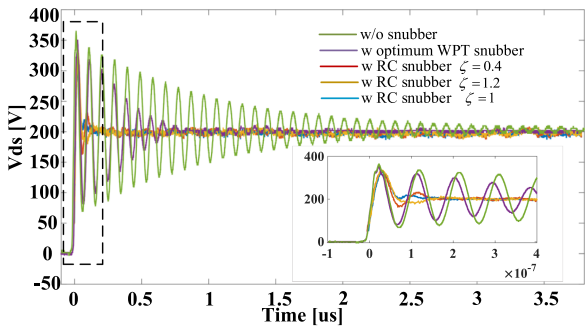

Fig. 11. Experimental waveforms of V_{ds} w/o WPT and *RC* snubbers.

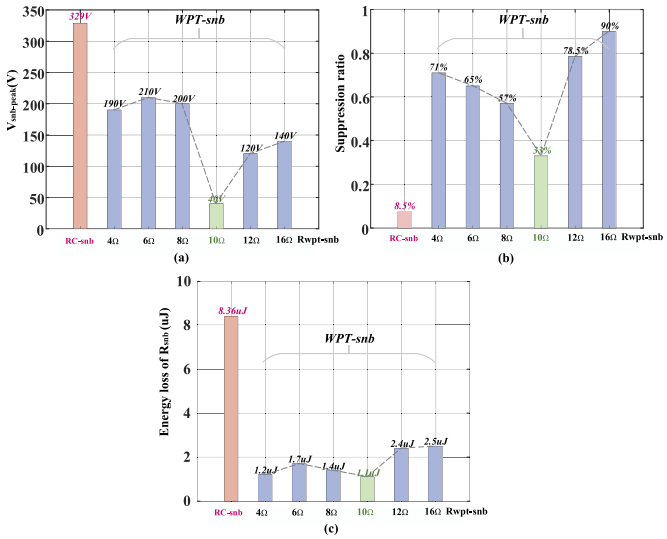

Fig. 12. Compare the three evaluation criteria of *RC* snubber and WPT snubber. (a) Permissible voltage. (b) Suppression ratio. (c) Energy loss.

8.5% ($\zeta = 1$) whereas, WPT snubber reduces it to 33%. However, according to formula (9), although ringing can be significantly suppressed with an increase in C_{snb}, there is a significant increase in loss P_{snb}. Therefore, compared to *RC* snubber, WPT snubber has greater advantages in reducing switching energy of R_{snb} and requiring less permissible voltage of capacitor. In addition, Fig. 12 displays three distinct evaluation criteria for analyzing and selecting the optimal $R_{\text{wpt-snb}}$. The metrics for evaluation include permissible voltage of $C_{\text{wpt-snb}}$, the ringing suppression ratio, and the power dissipation of $R_{\text{wpt-snb}}$. The ringing suppression ratio is a measure of the end time of switch ringing with a snubber circuit compared to the end time without any snubber circuit. After conducting a comprehensive comparison, it can be concluded that when $R_{\text{wpt-snb}}$ is set to 10 Ω, $C_{\text{wpt-snb}}$ exhibits the minimum permissible voltage, the maximum suppression ratio, and the smallest power dissipation of $R_{\text{wpt-snb}}$. Notably, the oscillation time of ringing can be shortened to 33% in Fig. 12(b). Compared to *RC* snubber, permissible voltage of $C_{\text{wpt-snb}}$ is reduced by 87.84%, and energy loss of $R_{\text{wpt-snb}}$ is reduced by 86.84%, as shown in Fig. 12(a) and (c).

IV. Conclusion

In this letter, a novel WPT snubber circuit to mitigate SiC MOSFET ringing caused by parasitic impedances is proposed. The circuit transfers ringing energy to a receiver via magnetic resonant coupling, reducing oscillation time by up to 67%. Moreover, compared to the traditional *RC* snubber circuit, the WPT snubber circuit naturally possesses electrical isolation, and its passive components do not have to withstand high turn-OFF voltage, causing a huge improvement of power density.

References

[1] T. Liu, R. Ning, T. T. Y. Wong, and Z. J. Shen, "Modeling and analysis of SiC MOSFET switching oscillations," *IEEE J. Emerg. Sel. Topics Power Electron.*, vol. 4, no. 3, pp. 747–756, Sep. 2016.

[2] Y. Wu, S. Yin, H. Li, and W. Ma, "Impact of RC snubber on switching oscillation damping of SiC MOSFET with analytical model," *IEEE J. Emerg. Sel. Topics Power Electron.*, vol. 8, no. 1, pp. 163–178, Mar. 2020.

[3] C. Yang, Y. Pei, L. Wang, L. Yu, F. Zhang, and B. Ferreira, "Overvoltage and oscillation suppression circuit with switching losses optimization and clamping energy feedback for SiC MOSFET," *IEEE Trans. Power Electron.*, vol. 36, no. 12, pp. 14207–14219, Dec. 2021.

[4] W. Han, K. T. Chau, and Z. Zhang, "Flexible induction heating using magnetic resonant coupling," *IEEE Trans. Ind. Electron.*, vol. 64, no. 3, pp. 1982–1992, Mar. 2017.

[5] "Designing RC snubbers," in Nuts & Volts Magazine Rev.1, Apr. 2012. [Online]. Available: https://www.nutsvolts.com/uploads/wygwam/AN11160_Designing_RC_Snubbers__NXP.pdf

[6] J. Zhou, B. Zhang, W. Xiao, D. Qiu, and Y. Chen, "Nonlinear parity-time-symmetric model for constant efficiency wireless power transfer: Application to a drone-in-flight wireless charging platform," *IEEE Trans. Ind. Electron.*, vol. 66, no. 5, pp. 4097–4107, May 2019.